


Article

# LiDonit<sup>®</sup>—A Potential Secondary Raw Material for Ceramic Applications in Concentrated Solar Energy

Gözde Alkan <sup>1,\*</sup>, Peter Mechnich <sup>1</sup>  and Johannes Pernpeintner <sup>2</sup><sup>1</sup> German Aerospace Center, Institute of Materials Research, 51147 Cologne, Germany; peter.mechnich@dlr.de<sup>2</sup> German Aerospace Center (DLR), Institute of Solar Research, 51147 Cologne, Germany; johannes.pernpeintner@dlr.de

\* Correspondence: goezde.alkan@dlr.de

**Abstract:** Solid particles as heat absorptances and storage mediums promise enhanced energy storage densities in concentrated solar power/thermal (CSP/T) plants. Employment of metallurgical slags as a secondary precursor material for solid particle preparation is ecologically and economically beneficial. Although these processed wastes, comprised of several oxides, exhibit generally promising high-temperature properties, chemical scattering from batch to batch may result in distinct material and functional properties, which may be an obstacle for their utilization. In this study, a steelmaking slag, LiDonit (LD), produced using a unique controlled slag treatment with high reproducibility is investigated as a candidate material. The aforementioned subsequent unique slag treatment makes LD a very promising and distinguishable secondary raw material for high-temperature applications. The as-received microstructure, phase components, and chemical composition of the LD material were analyzed to understand its material properties and to assess its reproducibility. The as-received LD chunks were transferred into pellets by subsequent milling, gel-casting, and sintering stages to reveal the potential processing routes. The CSP/T-related properties of sintered pellets, such as high temperature stability, heat capacity, and solar absorptance, were also examined to reveal their potential use in CSP/T applications and expand application areas with high added value.

**Keywords:** concentrating solar power; solar energy; metallurgical slags; secondary resources

**Citation:** Alkan, G.; Mechnich, P.; Pernpeintner, J. LiDonit<sup>®</sup>—A Potential Secondary Raw Material for Ceramic Applications in Concentrated Solar Energy. *Minerals* **2024**, *14*, 752. <https://doi.org/10.3390/min14080752>

Academic Editor: M Akbar Rhamdhani

Received: 27 May 2024

Revised: 11 July 2024

Accepted: 22 July 2024

Published: 26 July 2024



**Copyright:** © 2024 by the authors. Licensee MDPI, Basel, Switzerland. This article is an open access article distributed under the terms and conditions of the Creative Commons Attribution (CC BY) license (<https://creativecommons.org/licenses/by/4.0/>).

## 1. Introduction

Utilizing renewable energy technologies and providing a sustainable energy supply is crucial to decarbonize industrial processes and reduce greenhouse gas emissions. Thermal energy storage (TES) system integrated concentrated solar power (CSP/T) technology is considered to be one of the most efficient green energy methods [1,2]. The development of solid particle solar receivers (SPSR) and their integration into concentrated solar power plants (CSP) promise enhanced solar-to-electricity efficiency and a significantly reduced cost level of electricity, owing to the advantages of solid particle technology [3–5]. The utilization of high-temperature stable ceramic particles as heat absorbers and storage mediums promises higher operational temperatures (1000 °C), larger temperature ranges, and higher storage densities at low costs with respect to molten salt systems [6]. State-of-the-art solid particles are considered to be fracking industry bauxite proppants, owing to their good sphericity, solar absorbance, and thermal shock resistance [7]. Despite the aforementioned advantages, bauxite proppants may exhibit scattering functional properties due to the varying chemical composition of raw materials [8]. Moreover, after a long time exposure to high temperatures, a significant loss of optical properties due to the instable surface structures are reported, which makes their long-term use inefficient [8,9]. Therefore, there are still many studies aiming to modify state-of-the-art proppants and develop new compositions [10–13].

The utilization of industrial process wastes, specifically metallurgical slags, as precursors for heat absorbance and storage medium materials offers economic and ecological

benefits [14,15]. Considering the growing annual industrial waste production rates in Mt scale, any kind of use of these materials serves waste management, which is becoming more and more challenging [14]. These metallurgical process wastes comprise an appreciable amount of oxides, which offer promising high-temperature structural and functional properties relevant for CSP/T in particular [16–18]. There have been already several studies assessing non-ferrous and ferrous slags as heat storage materials, where promising properties were reported [16,19,20]. In a study conducted by Fai et al., the importance of crystal degree was emphasized to achieve the desired thermophysical properties with fly ash and asbestos wastes [21]. In recent studies, the importance of crystallization on the solar absorptance of fly ash was revealed by Glosser et al. [22]. Glosser et al. also investigated the effect of the oxidizing/inert atmosphere of thermal cycling on solar absorptance [23]. There are also several studies investigating the high-temperature properties of copper slag, revealing high heat capacity, thermal conductivity, and thermal stability [24,25]. In a recent study, copper slags were also reported as promising high-temperature phase change materials for thermal energy storage applications [26]. In our previous work, we examined copper and lead production fayalitic slags in a comparative manner. State-of-the-art-like particles were prepared using those slags as precursors, with an average size of 1 mm. Very promising heat capacity, solar absorptance, and high-temperature properties were reported, and in parallel with Fai et al., the importance of crystallization on CSP/T-related functional properties was reported [27]. In a recent study conducted by Lai et al., several coal slags were investigated in terms of their density, thermophysical properties, and thermal stability, where the importance of chemical composition and crystal degree for desired properties were emphasized [28].

Although there are several promising preliminary results on slag valorization, scattering chemical composition is an obstacle for reproducible properties. Moreover, their microstructure and crystallization degree may also alter depending on the deposition condition, aging, smelting conditions, and subsequent cooling rates, which make the employment of sustainable secondary raw materials for the manufacturing of engineering materials a challenge [29]. Lidonit (LD) is a synthetic calcium silicate-rich mineral, produced during the Linz-Donawitz steelmaking process as converter slag. The company ThyssenKrupp Steel conducts a unique liquid slag treatment by introducing silicate and pure oxygen to ensure the long-term stability of this product [30]. When compared with other steelmaking slags, the optimized liquid slag treatment makes it a promising and distinctive candidate. Currently, LD is mainly aimed to be used in construction industry as a substitute in concrete making [30]. In this novel study, for the first time, its potential use in CSP applications and processing routes to prepare high-value-added products are examined to expand its applications. Initially, the chemical composition, phase components, and microstructure of the as-received LD chunks were investigated. Milled LD dust was used as a precursor to prepare pellets by gel casting, with subsequent sintering. Microstructural and phase changes were analyzed among the chunk-to-sintered-pellet processing route. Moreover, LD pellets were characterized in terms of their CSP-relevant properties such as solar absorptance, heat capacity, and thermal-mechanical stability.

## 2. Materials and Methods

### 2.1. LiDonit

LiDonit chunks (mm to cm size) and powders (0–63 mm) were obtained from Thyssenkrupp MillServices & Systems GmbH, Oberhausen, Germany. LiDonit is a residual slag material originating from basic oxygen steelmaking, also commonly referred to as the Linz-Donawitz (“LD”) process, where basic fluxes, mainly from added CaO-rich additives, enhance steel purification. The special LiDonit process involves further addition of silica-rich sands, and results in less basicity and chemical stability of the LD slag.

## 2.2. Sample Preparation

In order to produce pellets, LiDonit powders (35%) were mixed with aqueous agar solution (2% agar) at 95 °C to form a stable suspension, which was then casted into a disk-shaped mold with 5 mm diameter to obtain pellet form. The casted pellets were dried at room temperature (RT) for 48 h. Subsequently, the as-dried pellets were sintered in air in a resistor-heated chamber furnace for 2 h at 1200 °C with a heating rate of 10 °C/min.

## 2.3. Characterization Methods

Crystal structure of the as-received powders and the phase changes after sintering at high temperature were monitored using X-ray powder diffraction (XRD; D8 Advance, Bruker AXS, Karlsruhe, Germany) using Cu-K $\alpha_{1,2}$  radiation between  $2\theta$  of 10°–70° with a step size of 0.01° and step time of 0.5 s. Digital optical microscopy (VHX 1000; Keyence Deutschland GmbH, Neu-Isenburg, Germany) was used to reveal the appearance of the as-received chunks.

Microstructural and chemical analyses were performed using scanning electron microscopy in secondary electron mode (Ultra 55, Zeiss, Oberkochen, Germany) and energy-dispersive spectroscopy (EDS; UltiMate, Oxford, UK). Prior to the SEM analysis, LD chunks and pellets were exposed to metallographic mounting, where they were embedded into hot mounting powder EOP black (ATM Qness GmbH, Mammelzen, Germany). After setting the epoxy black under 160 °C and 100 bar in a mounting press (Struers, CitoPress-30, Willich, Germany) cross-sections were ground and polished. Thermal reactions and weight changes were analyzed using simultaneous thermal analysis under a flowing synthetic air atmosphere (80% N<sub>2</sub>, 20% O<sub>2</sub>; flow rate 10 mL/min) (STA 409 F3 Jupiter with SiC-heated furnace, Netzsch, Selb, Germany). Heat capacity from RT to 1100 °C was determined under DSC under similar conditions, but using a Pt-heated furnace and the sapphire comparison method. For this, an 80 mg sintered disk with 5 mm diameter was measured versus a 100 mg single-crystalline  $\alpha$ -Al<sub>2</sub>O<sub>3</sub> disk (5 mm); C<sub>p</sub> was then calculated on the basis of NBS sapphire reference data.

In situ optical shape detection in a heating microscope (L74/HS/1600, Linseis, Selb, Germany) was employed to observe sintering-related volume effects and deduce suitable sintering temperatures for powder samples.

Spectral absorptance of LiDonit powders was measured in a Perkin Elmer Lambda 950 Spectrometer according to the method described by Gobereit et al. [10]. Evaluation of the solar weighted absorptance (ASTM 173d) was performed in the wavelength range from 320 nm to 2500 nm.

## 3. Results and Discussion

The surfaces of the as-received LD chunks were investigated using optical microscopy to reveal the mineral aggregates, crystals, and mineral texture, as given in Figure 1.

The optical microscope revealed that dark-gray LD chunks exhibit a homogenous and crystalline texture with a dull appearance. No obvious glassy regions were detected in the as-received chunks, indicating promising crystal quality. Beyond the dominant dark-gray grains, small white regions were also noticed across the surface. For microstructural details, cross-sections of the as-received chunks were elucidated using SEM, as represented in Figure 2.

The microstructural analysis represented in Figure 2 reveals the distinct morphologies of LD chunks. A core–shell-like structure, where a granular darker core is surrounded by brighter grains, can be observed in Figure 2a,d. It is also worthwhile to emphasize that the observed voids in Figure 2a represent the inherent porosity of the as-received chunks. In Figure 2d, it is also possible to observe the flocculation of finer grains into the globular core region. On the other hand, Figure 2b,c reveals a distinct morphology, where needle-like bright crystals are distributed through a dark matrix. The chemical composition of these various microstructural regions represented in Figure 2a–d were analyzed using EDS, as can be found in Figure 3.



Figure 1. As-received LD chunk.

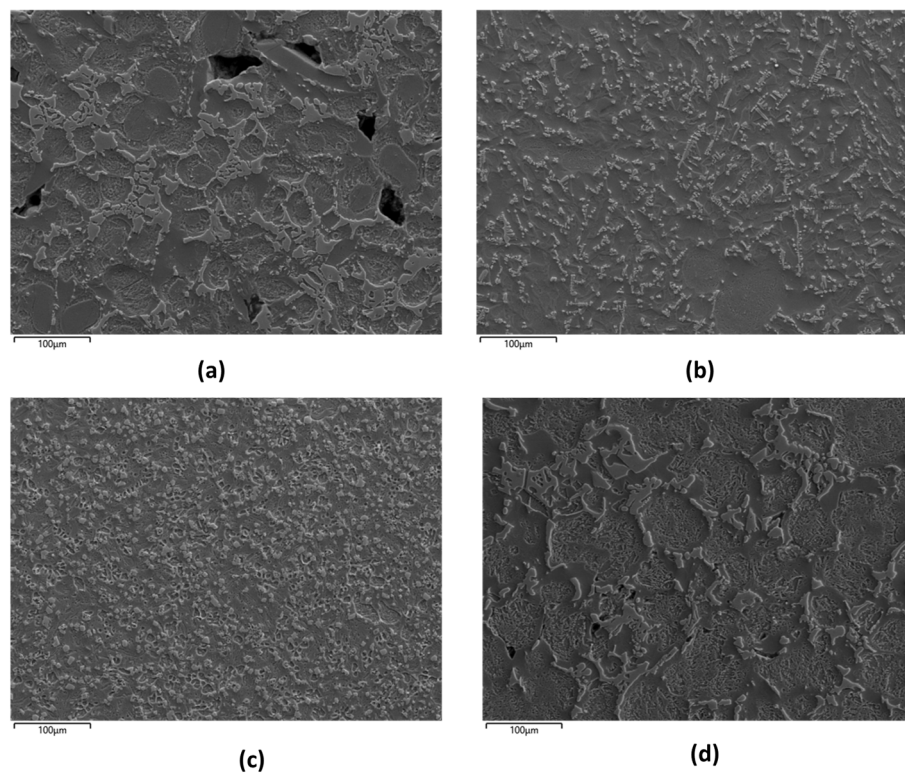
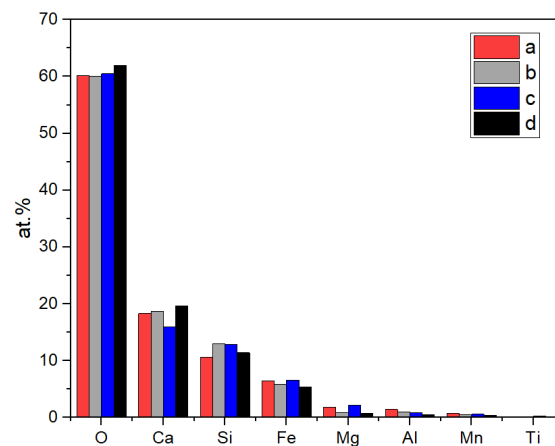


Figure 2. SEM microstructures of the as-received LD chunk cross-sections, revealing distinct morphologies (a,d) and granular core-shell-like (b,c) brighter needle-like crystals embedded in the darker matrix.



**Figure 3.** Chemical composition of the as-received LD chunks corresponding to SEM micrographs (Figure 2).

Figure 3 reveals the contents of each constituent element as measured using EDS analysis for four regions, with distinct microstructures given in Figure 2a–d. Unlike substantial microstructural variations, LD exhibits only limited chemical composition scattering, which favors its utilization as a chemically homogeneous raw material. Various morphologies may originate distinct cooling rates during the solidification of liquid slag [31]. The regions with a slower cooling rate may exhibit an equilibrium core–shell-like microstructure. A needle-like structure may be observed in the regions with fast cooling rates, where enough time for diffusion was not allowed [31]. Here, it is worthwhile to emphasize that the dominant microstructure of LD is the core–shell-like structure, and only minor regions exhibit the accompanying morphologies.

In order to identify the phase components of the as-received LD, an XRD analysis was performed, as plotted in Figure 4.

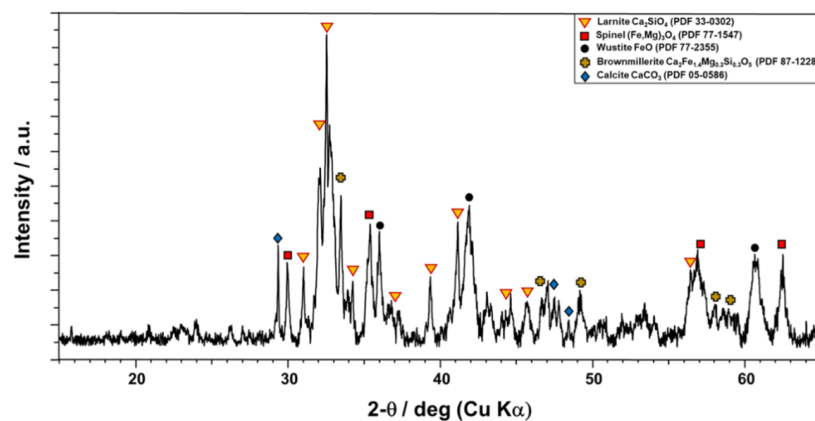


**Figure 4.** XRD diffractogram of the as-received LD powder.

Relative broad peaks may indicate the lack of crystallization or small crystals, which is common in metallurgical slags [32]. On the other hand, a variety of partially low-symmetry crystalline phases are detected which result in many overlapping low-intensity XRD peaks. One of the major phases of LD is larnite,  $\text{Ca}_2\text{SiO}_4$  (PDF 33-032). XRD analysis also indicates that two iron oxide polymorphs co-exist, a Wüstite-type iron monoxide ‘FeO’ (PDF 77-2355), and magnetite-type iron magnesium oxide  $(\text{Fe,Mg})_3\text{O}_4$  (PDF 77-1547), which may be due to the rapid cooling rates after steelmaking process. Further XRD peaks are well matched to a Brownmillerite-type phase such as  $\text{Ca}_2\text{Fe}_{1.4}\text{Mg}_{0.3}\text{Si}_{0.3}\text{O}_5$  (PDF 87-1228). XRD analysis also indicated the unexpected presence of a low amount of calcite,  $\text{CaCO}_3$  (PDF 05-0586), in the as-received LD material, which is discussed below. It is important to note that due to

the low crystal symmetry of constituents, many very low intensity peaks are occurring in the XRD pattern, and were not marked for better representation.

In order to reveal the chemical distribution of the microstructure, SEM/EDS mapping was performed in the LD cross-section, as given in Figure 5.

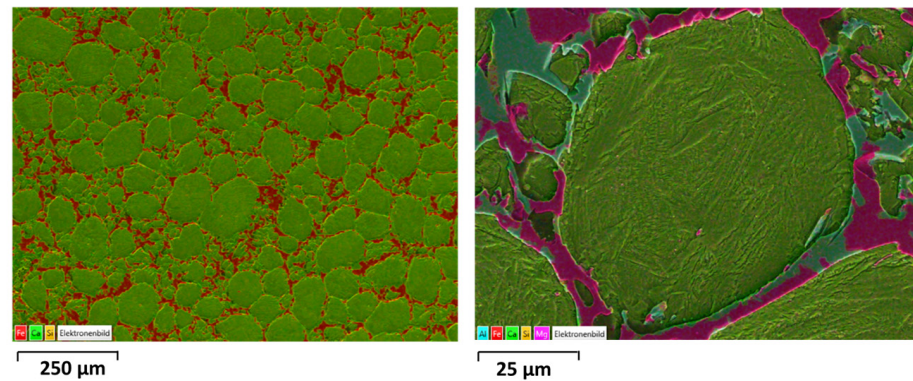


**Figure 5.** SEM/EDS Mapping of as-received LD chunk.

EDS mapping in Figure 5 reveals that the granular core region is enriched in terms of Ca and Si, which corresponds to the larnite phase detected using XRD (Figure 4). The surrounding shell-like regions comprised two phases, observed as Mg-rich and Ca-rich iron oxide regions, respectively. In light of the XRD findings, it can be said that magnetite- and Wüstite-type Fe-oxides and brownmillerite enclose globular larnite cores. Here, it is also worthwhile to emphasize that LD, even in its as-received form, exhibits a very well-crystallized microstructure, and almost no glassy phase was revealed, unlike most of the other metallurgical slags [32].  $\text{CaCO}_3$ , whose presence was indicated using XRD phase analysis, could not be observed in the SEM/EDS analyses of the cross-sections. However, a closer look at the surface using optical microscopy, presented in Figure 6, proves the presence of shiny white spots consisting of faceted crystals, which are evidently  $\text{CaCO}_3$ .

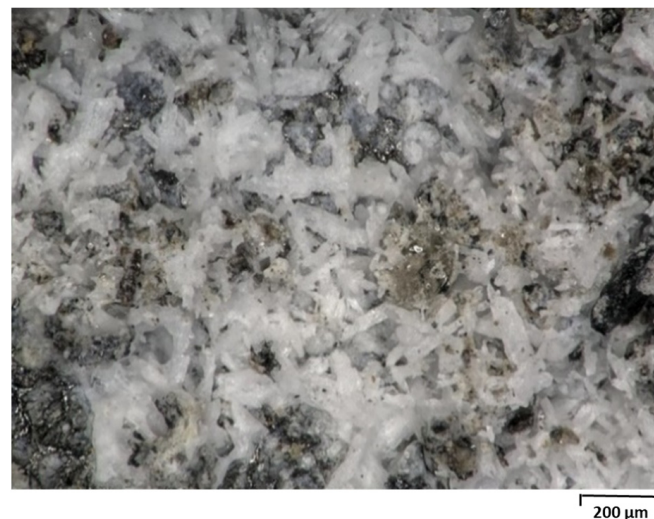


**Figure 6.** Appearance of the LD chunk's surface under an optical microscope.

As  $\text{CaCO}_3$  is evidently not stable in the molten LD slag, it is presumably formed with a reaction of free CaO with atmospheric  $\text{CO}_2$  after the cooling of the slag deposit.

After understanding the phase components and microstructure of the as-received LD, TGA and DSC analyses were performed to reveal its high-temperature properties and possible phase reactions, as given in Figure 7.

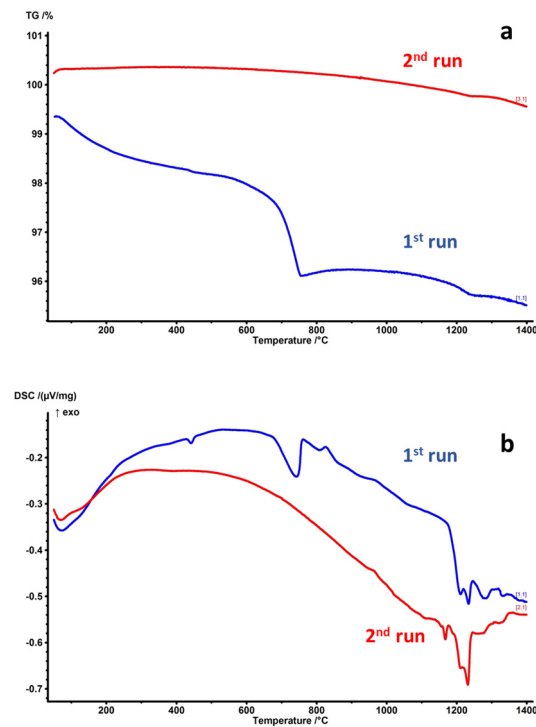


**Figure 7.** Thermal analysis of LD, and two subsequent runs from RT to 1400 °C at a heating rate of 10 K/min. **(a)** TGA. **(b)** DSC.

The DSC analysis shown in Figure 7a reveals that the as-received LD experiences several endothermic reactions upon heating, resulting in a significant mass loss. Upon first heating, mass loss starts gradually and becomes significant in the 600–800 °C temperature range, which can be assigned to  $\text{CaCO}_3$  decomposition, in parallel with XRD and optical microscopy findings. After calcination-related mass loss, upon first heating, the mass remains constant up to approximately 1000 °C, and afterward it is possible to observe a slight mass loss, which may be due to a partial reduction in the constituents, i.e., the release of oxygen. In the second heating ramp, a new small endothermic peak appears around 1150 °C, which may be the partial melting of a newly formed phase upon first heating. Large endothermic peaks observed upon both heating ramps around 1200 °C can be related to the extensive melting of their crystalline constituents, which is completed around 1300 °C. The melting in the 1200 °C temperature range can easily be attributed to the lowest ‘eutectic’ liquidus temperatures in the  $\text{CaO-SiO}_2\text{-FeO}_{1.5}$  system.

After comprehensive analysis on the as-received LD material, samples in pellet form were prepared using the gel-casting method. Using heating microscopy, the in situ shape change was investigated to determine the suitable temperatures for sintering LD powder compacts. The width of the pellet was recorded upon heating from RT to 1350 °C, as plotted in Figure 8.

The onset temperature of the sintering can be observed as 1150 °C in Figure 8. A maximum sintering velocity is reached at 1220 °C. As the temperature further increases, a plateau with low dimensional changes between 1230 and 1270 °C, but partial melting of the LD pellet and progressive wetting of the sample holder, was observed. Full melting was observed at around 1270 °C, in parallel with DSC findings. In order to obtain a well-consolidation of LD powder compacts and prevent the strong deformation due to the partial melting, 1200 °C was determined as the maximum sintering temperature. An LD pellet sintered at 1200 °C for 2 h was analyzed using XRD to reveal the phase composition, as plotted in Figure 9.

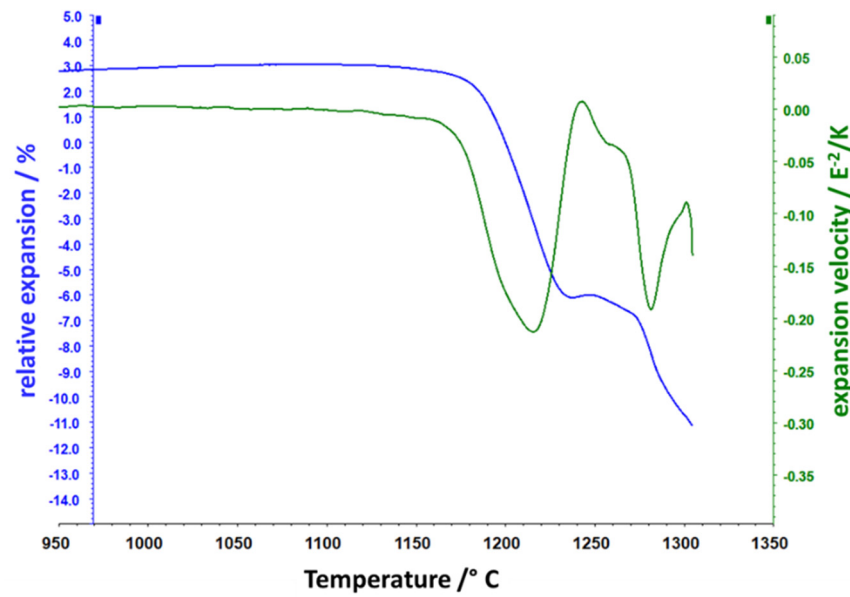


**Figure 8.** The relative height changes and derived sintering velocity of a gel-casted LD pellet during heating measured using heating microscopy up to 1350 °C (10 K/min).

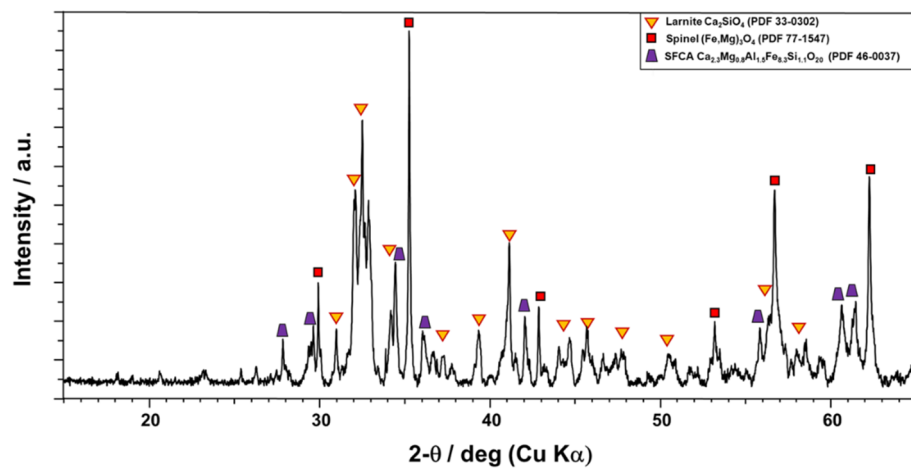


**Figure 9.** XRD diffractogram of an LD pellet sintered at 1200 °C for 2 h.

Figure 9 reveals the apparent change in the phase components of LD through sintering. Larnite and the corresponding granular core regions remain unaffected after sintering at 1200 °C. A significant increase in  $(\text{Fe,Mg})_3\text{O}_4$  peak intensities can be observed, while Wüstite-type FeO peaks have disappeared, implying that Wüstite is part of the metastable phase of the LD process which is stabilized as magnetite in  $\text{Fe}^{2+}$  to  $\text{Fe}^{3+}$  oxidation upon sintering. It is also evident that the brownmillerite phase disappeared after sintering, and a new phase well matching the XRD pattern of the ‘silico-ferrite of calcium and aluminum’ (SFCA) phase  $\text{Ca}_{2.3}\text{Mg}_{0.8}\text{Al}_{1.5}\text{Fe}_{8.3}\text{Si}_{1.1}\text{O}_{20}$  (PDF 46-0037) formed. SFCA-type solid solutions are commonly observed during iron ore sintering processes [33,34]. Actually, the newly found endothermic peak in the second heating DSC run may be caused by melting in this SFCA phase. Evidently, calcite completely disappeared, since sintering at 1200 °C ensures complete decomposition.

The microstructure and chemistry of the LD pellets sintered at 1200 °C were elucidated using SEM/EDS (Table 1), as given in Figure 10.



**Table 1.** Corresponding phase components of LD gel-casted pellets sintered at 1200 °C.

at. %	O	Ca	Fe	Si	Mg	Al	Mn	Phase
1	66.3	20	0.5	11.3	1.5	0.1	0.2	Larnite
2	61.6	0.8	24.1	0.1	8.5	1	3.5	Magnetite
3	63.8	6.2	22.1	2.8	1.6	2.2	1	SFCA

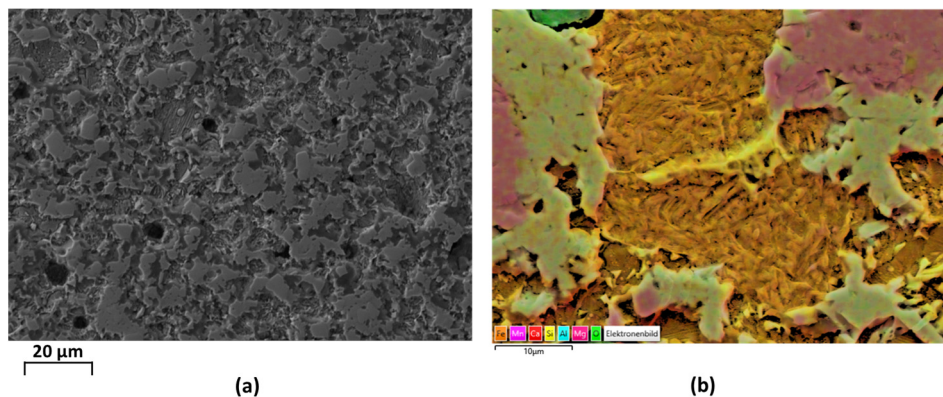


**Figure 10.** (a) SEM microstructure and (b) EDS mapping (close-up) of LD pellets sintered at 1200 °C for 2 h.

The SEM micrograph in Figure 10a reveals that sintering at 1200 °C ensured the consolidation of LD gel-casted pellets into a dense structure with a low amount of porosity. It is also possible to recognize the typical core–shell-like structure (Figure 2), even after milling, gel-casting, and sintering process steps. The as-received globular Larnite cores are conserved, whereas the surrounding layers include the newly formed SFCA phase, as also indicated using XRD and DSC/TGA analyses. Similar to the as-received condition, the surrounding layers also include a certain amount of magnetite-type spinel phase ((Fe,Mg,Mn)<sub>3</sub>O<sub>4</sub>). Similar to the well-crystallized LD starting material, the gel-casted and sintered LD pellets also exhibit a well-crystallized microstructure without glassy components, which is considered very promising for CSP-related properties.

After revealing the microstructural and phase changes through processing, LD pellets with optimized sintering conditions were evaluated in terms of their CSP/T-related functional properties. Heat capacity is considered to be one of the most important properties for solid particles and structural components employed in CSP/T technology, which ensures achieving enhanced energy storage densities. Figure 11 represents the temperature-dependent heat capacity of the LD-sintered tablet, measured using DSC analysis.

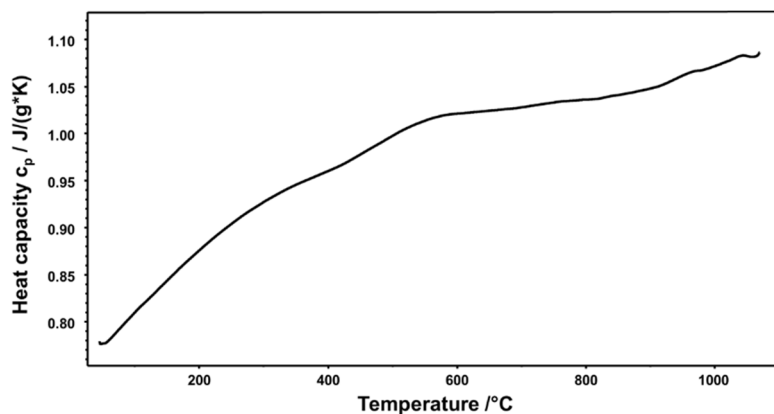


**Figure 11.** Temperature-dependent heat capacity of sintered LD pellets, as determined using the sapphire comparison method.

The LD pellet reaches a  $C_p$  value around 1 J/g-K around 900 °C, which is comparable with the  $C_p$  values of commercial solid particles used as heat absorptances and storage mediums [8]. A closer look reveals a discontinuity, i.e., slightly increasing  $C_p$  values beyond 900 °C, which is most likely explained by the redox reactions of iron oxide phases, as follows: since  $C_p$  values are calculated using the comparison method assuming constant sample masses, the presence of redox reactions resulting in slight mass changes, as observed in the TGA analysis (Figure 4), and may result in such an artifact.

Figure 12 shows the absorptance spectrum of an LD pellet sintered at 1200 °C for 2 h between 320 and 2500 nm, measured using spectrometry. According to the ASTM 173d standard, the solar-weighted absorptance of the LD pellet was calculated as 0.82, which is comparable with those of commercial state-of-the-art bauxite proppants and iron oxide granulates [12]. As revealed by the SEM and XRD results, the well-crystallized microstructures and the incorporation of Fe into SFCA and magnetite-type phases yields promising solar absorptance values, which makes LD a good candidate material for this application.

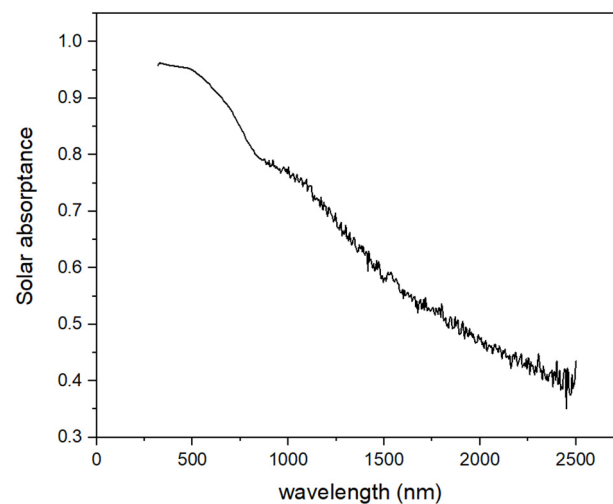


**Figure 12.** Solar absorptance of sintered LD material.

#### 4. Conclusions

LiDonit, a calcium silicate-rich steelmaking slag with reproducible chemical composition produced using a controlled slag treatment process was assessed as a candidate secondary raw material for use as a solar heat absorber and storage media. The XRD and SEM/EDS analyses on several as-received LD chunks produced in several batches revealed their controlled chemistry without significant scatterings, which makes LD a promising raw material candidate. Well-consolidated LD pellets can be prepared by milling, gel-casting, and sintering LD powders at 1200 °C. Despite its high Si content, well-crystallization into larnite without a significant glass-phase formation resulted in high temperature stability. Moreover, the relatively high content of color-giving Fe-Oxide and its stabilization in well-crystallized magnetite-type and SFCA-type phases also resulted in favorable solar absorptance around 0.82. The good heat capacity around 1 J/g-K at elevated temperatures also promises favorable heat storage densities. These preliminary experiments show that LiDonit is a very promising raw material candidate to prepare high-temperature stable ceramic products for CSP/T, particularly solid particles. It is possible to tune CSP-related functional properties by further adjustment in particle preparation and sintering steps. In future studies, thermal cycling tests, where particles are exposed to fast heating and cooling rates between 300 and 1000 °C, will allow us to estimate their lifetime in applicable near-conditions.

**Author Contributions:** Conceptualization, G.A. and P.M.; methodology, G.A. and P.M.; investigation, G.A., P.M. and J.P.; data curation, G.A. and P.M.; writing—original draft preparation, G.A. and P.M.; writing—review and editing, G.A. and P.M.; supervision, P.M. All authors have read and agreed to the published version of the manuscript.

**Funding:** This research received no external funding.

**Data Availability Statement:** Data are contained within the article.

**Acknowledgments:** The authors would like to thank Michael Dohlen (ThyssenKrupp MillService & Systems, Oberhausen, Germany) for the providing the Lidonit material and fruitful discussions.

**Conflicts of Interest:** The authors declare no conflicts of interest.

## References

1. Sarbu, I.; Sebarchievici, C. A Comprehensive Review of Thermal Energy Storage. *Sustainability* **2018**, *10*, 191. [\[CrossRef\]](#)
2. Barrasso, M.; Langella, G.; Amoresano, A.; Iodice, P. Latest Advances in Thermal Energy Storage for Solar Plants. *Processes* **2023**, *11*, 1832. [\[CrossRef\]](#)
3. Nie, F.; Bai, F.; Wang, Z.; Li, X.; Yang, R. Solid particle solar receivers in the next-generation concentrated solar power plant. *EcoMat* **2022**, *4*, e12207. [\[CrossRef\]](#)
4. Buck, R.; Giuliano, S. Solar Tower System Temperature Range Optimization for reduced LCOE. *AIP Conf. Proc.* **2019**, *2126*, 030010.
5. Palacios, A.; Barreneche, C.; Navarro, M.E.; Ding, Y. Thermal Energy Storage Technologies for Concentrated Solar Power—A Review from a Materials Perspective. *Renew. Energy* **2020**, *156*, 1244–1265. [\[CrossRef\]](#)
6. Calderón, A.; Barreneche, C.; Palacios, A.; Segarra, M.; Prietto, C.; Rodriguez-Sanchez, A.; Fernandez, A.I. Review of solid particle materials for heat transfer fluid and thermal energy storage in solar thermal power plants. *Energy Storage* **2019**, *1*, e63. [\[CrossRef\]](#)
7. Siegel, N.; Gross, M.; Ho, C.; Phan, T.; Yuan, J. Physical Properties of Solid Particle Thermal Energy Storage Media for Concentrating Solar Power Applications. *Energy Procedia* **2014**, *49*, 1015–1023. [\[CrossRef\]](#)
8. Alkan, G.; Mechnich, P.; Barbri, H.; Flucht, F.; Sergeev, D.; Müller, M. Evaluation of Ceramic Proppants as Heat Transfer and Storage medium. In Proceedings of the 27th SolarPACES Conference, Online, 27 September–1 October 2021.
9. Roop, J.; Jeter, S.; Abdel-Khalik, S.; Ho, C. Optical properties of select particulates after high-temperature treatment exposure. In Proceedings of the 8th International Conference on Energy Sustainability, Boston, MA, USA, 30 June–2 July 2014.
10. Gobereit, B.; Amsbeck, L.; Happich, C.; Schmücker, M. Assessment and improvement of optical properties of particles for solid particle receiver. *Sol. Energy* **2020**, *199*, 844–851. [\[CrossRef\]](#)
11. Alkan, G.; Mechnich, P.; Pernpeinter, J. Improved Performance of Ceramic Solar Absorber Particles Coated with Black Oxide Pigment Deposited by Resonant Acoustic Mixing and Reaction Sintering. *Coatings* **2022**, *12*, 757. [\[CrossRef\]](#)
12. Alkan, G.; Mechnich, P.; Pernpeinter, J. Using an Al-Incorporated Deep Black Pigment Coating to Enhance the Solar Absorptance of Iron Oxide-Rich Particles. *Coatings* **2023**, *13*, 1925. [\[CrossRef\]](#)
13. Farchado, M.; Vicente, G.S.; Barandica, N.; Sutter, F.; Alkan, G.; Sánchez-Señorán, D.; Morales, Á. Performance improvement of CSP particle receivers by depositing spinel absorber coatings. *Sol. Energy Mater. Sol. Cells* **2024**, *266*, 112681. [\[CrossRef\]](#)
14. Erregueragui, Z.; Tizliouine, A.; Ouhsaine, L.; Chafi, M.; El Hachami Omari, L. Selection and performance evaluation of waste and by-product materials for thermal storage applications. *Int. J. Low Carbon Technol.* **2022**, *17*, 888–899. [\[CrossRef\]](#)
15. Ferber, N.L.; Pham, M.D.; Falcoz, Q.; Meffre, A.; Tessier-Doyen, N.; Nzihou, A.; Goetz, V. Ceramics from municipal waste incinerator bottom ash and wasted clay for sensible heat storage at high temperature. *Waste Biomass Valorization* **2020**, *11*, 3107–3120. [\[CrossRef\]](#)
16. Gutierrez, A.; Miró, L.; Gil, A.; Rodríguez-Aseguinolaza, J.; Barreneche, C.; Calvet, N.; Py, X.; Inés Fernández, A.; Grágeda, M.; Ushak, S.; et al. Advances in the valorization of waste and by-product materials as thermal energy storage (TES) materials. *Renew. Sustain. Energy Rev.* **2016**, *59*, 763–783. [\[CrossRef\]](#)
17. Wang, Y.; Wang, Y.; Li, H.; Zhou, J.; Cen, K. Thermal properties and friction behaviors of slag as energy storage material in concentrate solar power plants. *Sol. Energy Mater. Sol. Cells* **2018**, *182*, 21–29. [\[CrossRef\]](#)
18. Krüger, M.; Haunstetter, J.; Knödler, P.; Zunft, S. Slag as an Inventory Material for Heat Storage in a Concentrated Solar Tower Power Plant: Design Studies and Systematic Comparative Assessment. *Appl. Sci.* **2019**, *9*, 1833. [\[CrossRef\]](#)
19. Ortega-Fernández, I.; Calvet, N.; Gil, A.; Rodríguez-Aseguinolaza, J.; Faik, A.; D’Aguanno, B. Thermophysical characterization of a by-product from the steel industry to be used as a sustainable and low-cost thermal energy storage material. *Energy* **2015**, *89*, 601–609. [\[CrossRef\]](#)
20. Fernandez-Gonzalez, D.; Pinuela-Noval, J.; Gomez-Rodríguez, C.; Fernandez Valdes, A.; Verdeja Gonzalez, L.F. Implications of renewable energy sources in metallurgy: Utilization of concentrated solar energy in recycling metallurgical wastes. *Appl. Therm. Eng.* **2024**, *250*, 123511. [\[CrossRef\]](#)
21. Faik, A.; Guillot, S.; Lambert, J.; Veron, E.; Ory, S.; Bessada, C.; Echegut, P.; Py, X. Thermal storage material from inertized wastes: Evolution of structural and radiative properties with temperature. *Sol. Energy* **2012**, *86*, 139–146. [\[CrossRef\]](#)

22. Glosser, D.; Striby, P.; Bellusci, M.; Bottem, R.; Amroun, S.; Suraneni, P. Characterization of optical and physiochemical properties of reclaimed fly ash for use as sensible thermal energy storage material in concentrating solar power systems. *Sol. Energy* **2023**, *263*, 111944. [[CrossRef](#)]
23. Glosser, D.; Bellusci, M.; Oos, K.; Johnson, D.; Suraneni, P. Solar absorptance of fly ashes cycled in oxidizing and non-oxidizing high temperature conditions. *J. Energy Storage* **2024**, *94*, 112487. [[CrossRef](#)]
24. Calderon-Vasquez, I.; Segovia, V.; Cardemil, J.M.; Barraza, R. Assessing the use of copper slags as thermal energy storage material for packed-bed systems. *Energy* **2021**, *227*, 120370. [[CrossRef](#)]
25. Navarro, M.E.; Martinez, M.; Gil, A.; Fernandez, A.I.; Cabeza, L.F.; Olives, R.; Py, X. Selection and characterization of recycled materials for sensible thermal energy storage. *Sol. Energy Mater. Sol. Cells* **2012**, *107*, 131–135. [[CrossRef](#)]
26. Ye, C.; Zhang, M.; Yang, S.; Mweemba, S.; Huang, A.; Liu, X.; Zhang, X. Application of copper slags in encapsulating high-temperature phase change thermal storage particles. *Sol. Energy Mater. Sol. Cells* **2023**, *254*, 112257. [[CrossRef](#)]
27. Alkan, G.; Mechnich, P.; Lucas, H.; Knoblauch, N.; Sommerfeld, M.; Flucht, F.; Pernpeintner, J.; Sergeev, D.; Müller, M.; Friedrich, B. Assessment of Metallurgical Slags as Solar Heat Absorber Particles. *Minerals* **2022**, *12*, 121. [[CrossRef](#)]
28. Lai, Z.; Cen, K.; Zhou, H. Applicability of coal slag for application as packed bed thermal energy storage materials. *Sol. Energy* **2022**, *236*, 733–742. [[CrossRef](#)]
29. Jonczy, I. Microstructures of Metallurgical Slags. *Arch. Metall. Mater.* **2016**, *61*, 61–66. [[CrossRef](#)]
30. Schlackenmanagement, LiDonit®. thyssenkrupp MillServices & Systems GmbH: Oberhausen, Germany.
31. Wu, L.; Li, H.; Mei, H.; Rao, L.; Wang, H.; Lv, N. Generation, utilization, and environmental impact of ladle furnace slag: A minor review. *Sci. Total Environ.* **2023**, *895*, 165070. [[CrossRef](#)]
32. Aysal, N.; Kurt, Y.; Öztürk, H.; Ildiz, G.O.; Yesiltas, M.; Laçin, D.; Öngen, S.; Nikitin, T.; Fausto, R. Crystallization Kinetics: Relationship between Crystal Morphology and the Cooling Rate—Applications for Different Geological Materials. *Crystals* **2023**, *13*, 1130. [[CrossRef](#)]
33. Webster, N.A.S.; Pownceby, M.I.; Madsen, I.C.; Studer, A.J.; Manuel, J.R.; Kimpton, A.K. Fundamentals of Silico-Ferrite of Calcium and Aluminum (SFCA) and SFCA-I Iron Ore Sinter Bonding Phase Formation: Effects of CaO:SiO<sub>2</sub> Ratio. *Metall. Mater. Trans. B* **2014**, *45*, 2097–2105. [[CrossRef](#)]
34. Kahlenberg, V.; Krüger, H.; Tribus, M.; Anwander, B. SFCA-II type Ca<sub>2.46</sub>Fe<sub>8.57</sub><sup>3+</sup>Fe<sub>0.52</sub><sup>2+</sup>Al<sub>5.45</sub>O<sub>24</sub>—An improved structural model for an iron-ore sinter phase. *Mineral. Petrol.* **2021**, *115*, 137–147. [[CrossRef](#)]

**Disclaimer/Publisher’s Note:** The statements, opinions and data contained in all publications are solely those of the individual author(s) and contributor(s) and not of MDPI and/or the editor(s). MDPI and/or the editor(s) disclaim responsibility for any injury to people or property resulting from any ideas, methods, instructions or products referred to in the content.